DETERMINING THE EFFECTS OF NON-CATASTROPHIC NAIL PUNCTURE ON THE OPERATIONAL PERFORMANCE AND SERVICE LIFE OF SMALL SOFT CASE COMMERCIAL LI-ION PRISMATIC CELLS

by

Casey Jones

A Thesis

Submitted to the Faculty of Purdue University

In Partial Fulfillment of the Requirements for the degree of

Master of Science in Aeronautics and Astronautics

School of Aeronautics and Astronautics

West Lafayette, Indiana

December 2020

THE PURDUE UNIVERSITY GRADUATE SCHOOL
STATEMENT OF COMMITTEE APPROVAL

Dr. Vikas Tomar, Chair

School of Aeronautics and Astronautics

Dr. J. Eric Dietz

School of Computer and Information Technology

Dr. Tyler Tallman

School of Aeronautics and Astronautics

Approved by:

Dr. Gregory A. Blaisdell

Dedicated to my parents, who have always supported everything I do.

ACKNOWLEDGMENTS

I would like to acknowledge the Office of Naval Research for their financial support of this research. I would also like to acknowledge both Veterans to Energy Careers and the Purdue Military Research Initiative for the research opportunities and support they have provided.

TABLE OF CONTENTS

LIST OF TABLES

LIST OF FIGURES

ABSTRACT

This work developed a novel experiment in order to determine the operational effects on a Lithium-ion battery (LIB) when a test resulting in non-catastrophic damage is performed. Accepted industry standards were used as a basis to develop a nail penetration test that would puncture a cell approximately halfway through during normal cycling at a rate of 1C, then allow the cell to continue cycling to determine how its operation was affected. The cells under test continued cycling after the punctures, showing that the experiment would be able to provide useful information on the topic. The experiment was found to be successful in simulating the operation of a cell in an abusive environment, such as those seen in electric vehicles and aerospace applications.

The results of these experiments showed that a sharp increase in temperature is observed immediately after the puncture, similar to cells that underwent tests with full penetrations. The temperatures then slowly decreased during the first few cycles after the puncture as the generated heat was dissipated through convection. The experiments also showed that it is possible for a LIB under test to continue operating for a short time after being punctured. However, the capacity and useful life of the cells were greatly reduced. The initial capacity of each cell decreased by approximately 11% after the initial impact, then continued decreasing at an accelerated rate during the ensuing cycling. The lifetime of the cells was also greatly reduced, with each cell reaching its end of life within approximately 15-75 cycles after the punctures. An analysis of the incremental capacity curves of the cells indicated that accelerated aging occurred due to both a loss of active material and a loss of lithium inventory. The information gained from the experiments gives insight into the operation of cells that experience abusive environments and will be useful in designing improved control systems, as well as promoting the development of more robust testing and safety standards for different types of cells.

1. INTRODUCTION

The following research was developed from multiple operational testing standards currently in use for LIBs. Initially, nail penetration tests that fully penetrated cells in operation were performed to observe the thermal response in small prismatic cells and obtain information about the likelihood of thermal runaway occurring. The responses observed from these experiments were consistent with results found in the available literature for the same types of tests. However, it was observed that the standards for nail penetration tests were only concerned with full penetrations. Also, they focused solely on whether or not the nail penetration resulted in thermal runaway either during or immediately after the penetration. No information was found in the testing standards for the thermal response of a cell that experiences only a partial nail penetration, or about the requirements for or operational effects on a cell after this type of event where a cell may still be operational after being only partially damaged. While some thermal response information is available from individual tests involving only a partial penetration, a review of relevant sources did not indicate that any extensive research had been undertaken on the operation of cells after this type of test. Because this information was not yet available, it was decided that a new type of experiment should be developed to study this issue, which was based on the battery testing standards that were currently available.

The industry standards that were initially used were expanded upon to develop a test that would simulate the operation of a battery in an abusive environment after being only partially damaged. The experiment that was developed implemented a drop hammer with a nail attached that was released to puncture the cell, and rubber shims were used to stop the nail after penetrating approximately halfway into the battery. The cell was cycled at a rate of 1C prior to the puncture, and the puncture occurred at the end of the charge cycle when the cell held the most potential chemical energy. After the puncture, the cell would continue being cycled at the same rate as before.

The manuscript contained in Chapter 3 provides a detailed explanation of the experimental setup and procedure; effects on the physical characteristics, temperature, capacity, coulombic efficiency, and incremental capacity of the cell; and an explanation of the results using an incremental capacity analysis to determine the effects that results from the experiment. It was

found that a partial penetration causing an accelerated aging of a cell, which greatly reduces the capacity, performance, and lifetime of a cell.

2. LITERATURE REVIEW

Batteries have developed into an integral part of electrical power storage and distribution in recent years. Developments in technology have made them smaller, lighter, and more powerful, and projections show these trends of improvement will continue. While advancements can bring about improvements in batteries, they can also bring new challenges. LIBs have been shown to be the most advantageous of current types of batteries; their high energy and power densities, small size, and reasonable cost make them attractive for most applications. Unfortunately, their safety is compromised by the possibility of thermal runaway caused by different types of damage or misuse during normal operation.

Due to many recent and highly publicized incidents involving LIBs, most commonly in electric vehicles and cell phones, thermal runaway has become a major safety concern. Thermal runaway is a situation where the amount of heat generated in a battery is greater than the amount of heat that can be dissipated due to uncontrollable exothermic reactions, which can lead to fires and explosions [1]. Many different factors contribute to the likelihood and severity of thermal runaway: type of material, number of cycles, charge/discharge rate, environmental temperature, and many others. This review will focus on factors that affect the likelihood of thermal runaway, how thermal runaway begins and propagates, and consequences of thermal runaway, as well as methods of detection for use in possible future solutions.

The most common types of LIBs are Lithium Cobalt Oxide (LCO), which use LiCoO2 as their cathode material, Lithium Manganese Oxide (LMO), which use LiMn2O4 as their cathode material, and Lithium Nickel Manganese Cobalt Oxide (NMC), which use LiNi(x)Mn(y)Co(z)O2 (where $x + y + z = 1$) as their cathode material. While each of these materials are susceptible to thermal runaway, LCO batteries were found to be less stable and released more heat than both LMO and NMC batteries, likely due to the fact that LCO batteries released more oxygen when operating at higher temperatures. The state of charge (SOC) of the batteries was also a factor, as a battery with a higher SOC had more delithiated active material. This made the higher SOC batteries more reactive, causing a lower temperature necessary for the onset of thermal runaway to occur [1]. Despite having a higher propensity for thermal runaway, LCO batteries are the most common due to their higher power and energy densities.

Other material factors can increase the possibility of thermal runaway occurring. Batteries that used lithium hexafluorophosphate ($LiPF_6$) as an electrolyte were more susceptible to thermal runaway. Also, the presence of organic solids in LIBs causes a low activation energy and promotes initiation of thermal runaway, whereas isolated electrolyte salts cause a high activation energy and help to prevent the initiation of thermal runaway [2]. While these factors contributed to the likelihood of thermal runaway occurring, their effect was not as significant as the effect of the cathode material.

Physical characteristics and imperfections from manufacturing can also make thermal runaway more likely [3]. The number of charge and discharge cycles has a very large effect, as the amount of metal lithium deposition on the anode increases with the number of cycles. These depositions, also known as dendrites, are highly reactive reagents, and their reactions are intensified at lower temperatures. This is further exacerbated when a battery is at a high SOC, leading to lower cathode stability and higher oxygen release [4]. This release of oxygen, combined with the release of hydrogen as well, is a major reason for rupture, fire, and explosion of batteries during thermal runaway.

During thermal runaway, the amount of heat generated is dependent on five major contributing factors: electrolyte resistance, anode resistance, cathode resistance, cathode entropy changes, and anode entropy changes. Heat generation is also dependent on environmental factors like temperature, where a lower temperature causes a higher rate of heat generation. The largest contributing factor to heat generation is electrolyte resistance, followed by cathode resistance and then anode resistance [5]. While much information was gained through these studies, the rate of heat generation varied with time and did not follow any apparent behavior, making it difficult to generate predictive models.

In many cases thermal runaway can lead to a rupture of LIBs, even those employing vents for the release of gases. Single-vent batteries often failed due to their electrodes blocking the vents, and rupture generally occurred at the crimp components where the seal was the weakest. High capacity cells also produced more gas and subsequently higher pressures, causing a higher chance of rupture. Two-vent batteries were more adept at releasing pressure and rarely failed. They also caused a slower propagation of thermal runaway due to the gas being vented more quickly [6]. Cells that ruptured also had the possibility of releasing high-velocity projectiles, an uncommonly reported occurrence but a safety concern nonetheless.

Aside from increased temperature, some commonly reported consequences of thermal runaway are combustion and explosion. However, the likelihood of fires is low, with an estimated probability of one in one million to one in ten million. Usually, fire caused by thermal runaway is due to a short-circuit in a battery and its subsequent overheating. This causes the exothermic reaction to become uncontrollable, and the reaction rate and temperature simultaneously cause each other to increase. Heat generation becomes exponential while heat dissipation remains linear, and eventually the battery will combust or explode. Thermal runaway in a single cell can also cause a chain reaction in nearby cells, as some batteries pack cells close together to reduce overall size [7]. These cells also dissipate heat slower due to having less surface area, further increasing the likelihood of thermal runaway.

Many approaches to detecting thermal runaway are being studied as possible methods of prevention [8]. These methods are based on the examination of different factors such as voltage, temperature, pressure, creep distance, piezoresistive force, and the presence of gas or smoke. While sensor for each of these characteristics exhibited a distinct reaction to thermal runaway, there were clear differences in the effectiveness of their indications. The sensors for detecting gas and smoke responded the fastest to thermal runaway but were unstable and had the possibility for false indications. Sensors for creep distance and pressure had smoother responses but were slower than the gas and smoke sensors. While the temperature and voltage sensors were the slowest, they were also the most reliable [9]. While there was no definitive best sensor due to their different benefits and disadvantages, a combination of sensors could possibly be used to address all concerns and improve overall reliability.

New methods of analysis are contributing to the development of solutions for thermal runaway. Traditional research generally focuses on only a few factors at one time, whereas mathematical models can use a large number of factors to make more complex predictions of thermal behavior. These models can incorporate factors such as entropy, environmental temperature, and mean cell temperature. They can also scale up the size of batteries being studied, as this will lead to different complexities not usually seen in smaller batteries [10]. While these models are new and have yet to contribute much information, they are likely to be fundamental in finding solutions to prevent thermal runaway.

Damage due to mechanical abuse is a major factor that increases the probability of thermal runaway. Internal short circuits are the most common result of physical damage, which can be

easily and accurately simulated using pinch and pinch-torsion tests. Since batteries susceptible to this kind of damage are usually large, thin pouch cells, the pinch-torsion test is a better simulation. Results of these tests show that most batteries had little or no temperature increase after the pinch-torsion test was applied. However, those tested with a high SOC showed a significant temperature increase, usually resulting in thermal runaway [11]. This reinforces the notion that a high SOC is a major factor to increase the probability of thermal runaway.

Many different types of abuse have been adopted as the basis for testing the operational standards for LIBs. Methods such as overcharge, overcurrent, shock, impact, crush, vibration, thermal abuse, nail penetration, and immersion in saltwater have been implemented to determine the level of safety and performance requirements when using or transporting LIBs. However, these tests generally focus on whether or not a cell or battery pack under test undergoes thermal runaway, and most use a go/no-go criterion in their determination. Little research has been performed that focuses on the operational effects of these cells during sustained operation after the tests have been completed. Due to this knowledge gap, it is difficult to determine how to proceed with normal operation if a device or piece of equipment must continue operating after undergoing an event similar to these tests. It is also not known how these tests affect a cell or how long a cell will continue operating afterwards.

One of the most successful abuse methods used to study the thermal response in cells is the nail penetration test. The penetration of a nail into a cell causes an internal short circuit due to the pinching of the electrode layers. This internal short circuit leads to joule heating, which raises the temperature of the cell and increases the likelihood of thermal runaway. This helps to determine the stability of a cell when encountering a large amount of structural damage, but the method is limited due to the fact that the penetration releases gas and electrolyte which can alter the thermal response of the cell [12, 13]. Nail penetration simulations can correct for deficiencies and also include other factors relevant to thermal runaway, and these simulations have successfully been performed recently [14, 15].

Some research has recently been performed in order to determine how these types of abuse tests affect the morphology of a cell, though more research in the area is needed to provide conclusive results for the many different types of cells available [16, 17]. The initial indications are that abusing a cell will cause an acceleration in aging, which is suspected to lead to a reduction in capacity and shorter operational life [18]. Traditional methods such as Raman spectroscopy and

scanning electron microscopy have been used to determine the accelerated aging effects that these tests can have on cell morphology.

Recently, other nonintrusive methods of analysis have emerged that have proven to be highly accurate in determining the type and extent of aging in cells. The most commonly used method is the analysis of the incremental capacity curve of a cell. By observing the shift in both the maximum values and corresponding voltages of the different peaks of the incremental capacity curves, the methods of aging and their extent can be determined throughout the life of different cells [19, 20].

While advances in battery technology have brought many advantages in energy storage methods, there are still complications that must be addressed. As batteries improve, there are also likely to be many new and unforeseen obstacles as well. Though many challenges are likely to emerge in the future, current technology has shown great promise in being effective at detecting and preventing thermal runaway.

3. MANUSCRIPT IN-REVIEW: DETERMINING THE EFFECTS OF NON-CATASTROPHIC NAIL PUNCTURE ON THE OPERATIONAL PERFORMANCE AND SERVICE LIFE OF SMALL SOFT CASE COMMERCIAL LI-ION PRISMATIC CELLS

Casey Jones [a1], Bing Li [a1], Vikas Tomar [a*]
[a] School of Aeronautics and Astronautics, Purdue University, West Lafayette, IN 47907, USA
[1]: Equal contribution.
[*]: Corresponding author. Address: 701 W Stadium Ave, West Lafayette, IN 47907, USA. Email: tomar@purdue.edu
A version of this manuscript has been submitted to eTransportation for review.

3.1 Abstract

This work focused on the operational effects of Li-ion batteries (LIBs) that had been partially damaged and were allowed to continue operating afterwards. The intent was to simulate the operation of a damaged cell in an abusive environment, such as that found in electric vehicles and hybrid-electric vehicles. A test rig implementing a drop hammer with a nail attached was used to puncture approximately halfway through cycling LIBs to determine how their operation was affected. For all LIBs tested, the puncture caused a rapid spike in temperature. The dynamic impact immediately caused an initial drop in capacity of approximately 11%, and capacity continued to decrease throughout the remainder of the cycles. The cells also reached their end of life within an average of 43 cycles after the puncture, much sooner than the rated lifetime. Postmortem analysis of the punctured LIBs presented impact induced physical damage to the electrodes, oxidation of the electrolyte, and degradation of the interior components of the cells. This caused a decrease in discharge capacity and shortened useful lifetime due to hindering the charge capability of the cells. The degradation mechanism of the cells was further determined using peak tracking of the incremental capacity curves throughout their lifetimes.
Keywords: Lithium ion battery, dynamic impact, battery aging, destructive testing, capacity fade

3.2 Introduction

Lithium ion battery (LIB) technology has greatly advanced in recent years, improving the capacity and efficiency of electrochemical energy storage and distribution [1, 2]. Batteries have

become smaller and lighter with improved performance, allowing for greater design flexibility and operational use [3]. However, LIBs are chemically unstable when damaged and can become hazardous when operating in abusive conditions [4-6]. Electrical failures, mechanical agitation, impacts, and internal short circuits can lead to thermal runaway in batteries [7, 8]. In addition to the expected decline in operational performance caused by the structural damage of the cell, internal shorting of the electrodes caused by a nail penetration can lead to thermal runaway [9]. This can cause catastrophic failures of cells and battery packs such as increased temperatures, combustion, and possibly explosion [10-13].

When batteries are operating in extreme environments with abusive conditions, physical damage to cells by foreign materials becomes much more likely. These conditions are especially common in aerospace applications where planes can be put out of commission due to battery failures [14]. These conditions are also present in electric vehicles (EVs) and hybrid electric vehicles (HEVs), especially while driving on rough terrain or from damage caused by accidents [15]. A report issued by the National Transportation Safety Board (NTSB) concerning an EV crash showed that the fire that ensued after the crash was due to the EV's battery being breached [16]. In a study conducted by NTSB through Underwriters Laboratories, a nail penetration test was performed on Boeing 787 batteries to determine the effect on failure behavior after issues had been found in these batteries in 2013. The tests showed that nail penetrations caused short circuits within the cells, leading to heat generation that was transferred to nearby cells and caused ensuing short circuits in those cells also. This caused increased temperatures in each cell tested, as well as combustion and the emission of smoke and gas due to thermal runaway in some cells [17].

Many testing standards have been developed that simulate these types of damage by puncturing a cell with a nail. Most current testing standards specify that the nail must fully penetrate the cell during the test to observe if a catastrophic failure occurs. However, it is also possible that a cell could be only partially damaged by a foreign object during operation. This type of damage may only lead to a small puncture in the cell casing that does not affect all the electrode layers in the cell. This could allow a cell to remain operational even after being damaged, which has not been adequately addressed by recent research and is not covered by major current testing standards. Recent research has mainly concentrated on the thermal effects of cells that have been damaged beyond use, but has not focused on the possibility of a cell continuing to operate after being damaged [8, 18, 19]. Studies that monitored cell performance during abusive conditions

have noted accelerated capacity fade and decreased efficiency, as well as full penetrations being necessary to induce a failure event during nail penetration tests [9, 20]. Based on the possibility of cells experiencing only minor damage and continuing to operate, we designed a novel experiment to determine the immediate and long-term response of LIBs to nail punctures that do not destroy the batteries beyond the point where they are still operational. This experiment was developed by modifying the standards normally used for nail penetration tests to allow the tip of a nail to only penetrate halfway into an operating cell, then allow it to continue cycling after being damaged. The experiment was designed to simulate the operation of a cell in an abusive environment where continued operation may be possible after damage, and the results give greater insight into how cells operate after being partially damaged. This type of testing can simulate an abusive environment such as that seen in EVs where damage can lead to catastrophic failures [21, 22]. The effects of dynamic impact on small Li-ion prismatic cells were analyzed in terms of battery temperatures, capacity, coulombic efficiency, and incremental capacity. The results from the experiments showed that cells which experienced this type of damage exhibited highly increased capacity degradation and reached their end of life shortly after, showing that they were unreliable for use in long-term operation after such damage had occurred.

3.3 Method

3.3.1 Experiment Setup

Physical damage to individual cells and battery packs due to dynamic impact is a common occurrence in EV service. In cases of severe damage such as nail penetrations, cells normally lose operational ability and can encounter catastrophic failures such as thermal runaway and explosion. Mechanical abuse testing can provide useful information on how batteries respond to being physically damaged, which can vary widely depending on the type of battery and how it is damaged. However, most previous experiments have focused on damaging cells to the point of failure without determining their response to minor amounts of damage [22]. In field applications such as EVs, it is common that dynamic impact does not cause thermal runaway instantaneously, but the resulting damage to the structure of the batteries threatens their safe operation. NTSB has reported cases where EVs involved in traffic accidents did not catch fire immediately, but were ignited shortly after [23]. To study the effects of LIB damage from dynamic impact with limited

momentum, a novel non-catastrophic nail puncture test was designed to abuse the cells without triggering thermal runaway and analyze their operation afterwards. This experiment was developed based on the nail penetration tests in LIB safety standards developed by the United Nations [24], SAE International [25], and Sandia National Laboratories [26]. Nail penetration tests are important for collecting information on thermal propagation generated by an internal short circuit caused by a nail penetration with impact occurring in the direction most likely to cause thermal runaway (perpendicular to the electrodes in prismatic cells). For these nail penetration tests, the only information desired by the testing standards mentioned previously is whether or not thermal runaway occurs, and the cells under test are only monitored for long enough after the penetration to determine if thermal runaway does occur (about one hour). The standards for these nail penetration tests are shown in Table 1.

Table 1: Applicable nail penetration test standards from UNECE, SAE International, and Sandia National Laboratories.

	UNECE GTR No. 20	SAE J2464	Sandia FreedomCAR
Nail material	Steel	Mild conductive steel	Mild conductive steel
Nail diameter	3 mm or more	3 mm	3 mm
Nail end type	Circular cone, 20°-60° angle	Tapered to sharp point	N/A
Rate of penetration	0.1-10 mm/s	8 cm/s or greater	N/A
Penetration depth	N/A	Through cell	Through cell
Penetration orientation	Vertical direction to electrode layers	Perpendicular to electrodes	Perpendicular to electrodes
Nail removed after impact	N/A	No	N/A
Ambient temperature	25 °C ± 2 °C	Room temperature (25 C± 5 °C)	25 °C ± 5 °C
State of charge (SOC) at impact	Highest normal state per manufacturer	Fully charged (100%)	Fully charged (100%)

While these standards are useful in determining thermal responses of cells that are damaged to the point that they are no longer operational, they do not consider how the operation of a cell is affected by a dynamic impact that does not lead to the complete destruction of a cell. The experiment we developed required that the cells be monitored and their operational characteristics recorded before, during, and after the impact to determine how their operation was affected after

the damage occurred. Allowing the cells to maintain their ability to continue cycling was accomplished by limiting the depth of the nail upon impact to approximately halfway through the cell, which prevented catastrophically damaging all of the electrode layers. The cells were cycled 100 times after the puncture to reach 80% of their initial capacity, which is typically considered to be their end of life (EOL) [27-29]. The majority of the testing standards in Table 1 are similar with some minor differences in phraseology. Our experiment followed these standards with the exception of two major differences: the nail impact depth was 2 mm (approximately halfway through the cell) instead of completely through the cell, and the nail was removed after impact to prevent possible interference with the operation of the cell. Also, since the controlling factor for this experiment was the depth of penetration that would allow the cells to continue operating afterwards, the velocity was not considered in the experimental standards. A theoretical calculation of the velocity found the value to be approximately 35 cm^{-1}. This is expected to be higher than the standards for a full nail penetration test, as nail penetration tests require lower velocities in order to investigate the results at the time of impact. The nail penetration tests also use a continuous force to penetrate a cell with a nail, whereas the force from a drop hammer test is dependent on the initial height of the hammer. These changes allowed for only minor damage to occur to the cell being tested, which simulated a piece of debris damaging a cell during operation in an abusive environment. Since the impact momentum was limited, cycling continued after the puncture and information was provided on the operational performance of the partially damaged LIBs.

The LIBs used in the experiment were commercially available $LiCoO_2$ (LCO) prismatic cells manufactured by Powerizer, and their specifications are given in Table 2.

Table 2: Basic parameters of prismatic cells used in experimental testing.

Lab rated capacity (using 1C charge/discharge rate)	130 mAh
Nominal voltage	3.7 V
Charge voltage	4.2 V
Discharge cut-off voltage	3.0 V
Charging current	0.17 A Max.
Discharging current	0.34 A Max.
Cycle life	>500 cycles
PCM cutoff voltage	4.5 V/2.4 V
PCM max current	2 A

Four resistance temperature detectors (RTDs, Pt-1000 from Omega Engineering) were used for in-situ monitoring of the temperatures of the cells. Fig. 1 (a-d) show the placement of the RTDs on the cells, as well as the location and depth of the nail puncture. A protection circuit module (PCM, model PCB-S1A2 from AA Portable Power Corp.) was used during cycling to prevent overcharge, overdischarge, and overcurrent of the cells. Battery holders with holes in the center so the nail could pass through the top holder during impact were prepared with additive manufacturing of polylactic acid (PLA) to secure the experimental setup to the test rig and ensure proper contact between the cell and RTDs during impact. The two holders used were identical to allow for symmetric heat dissipation from the top and bottom of the cells during testing.

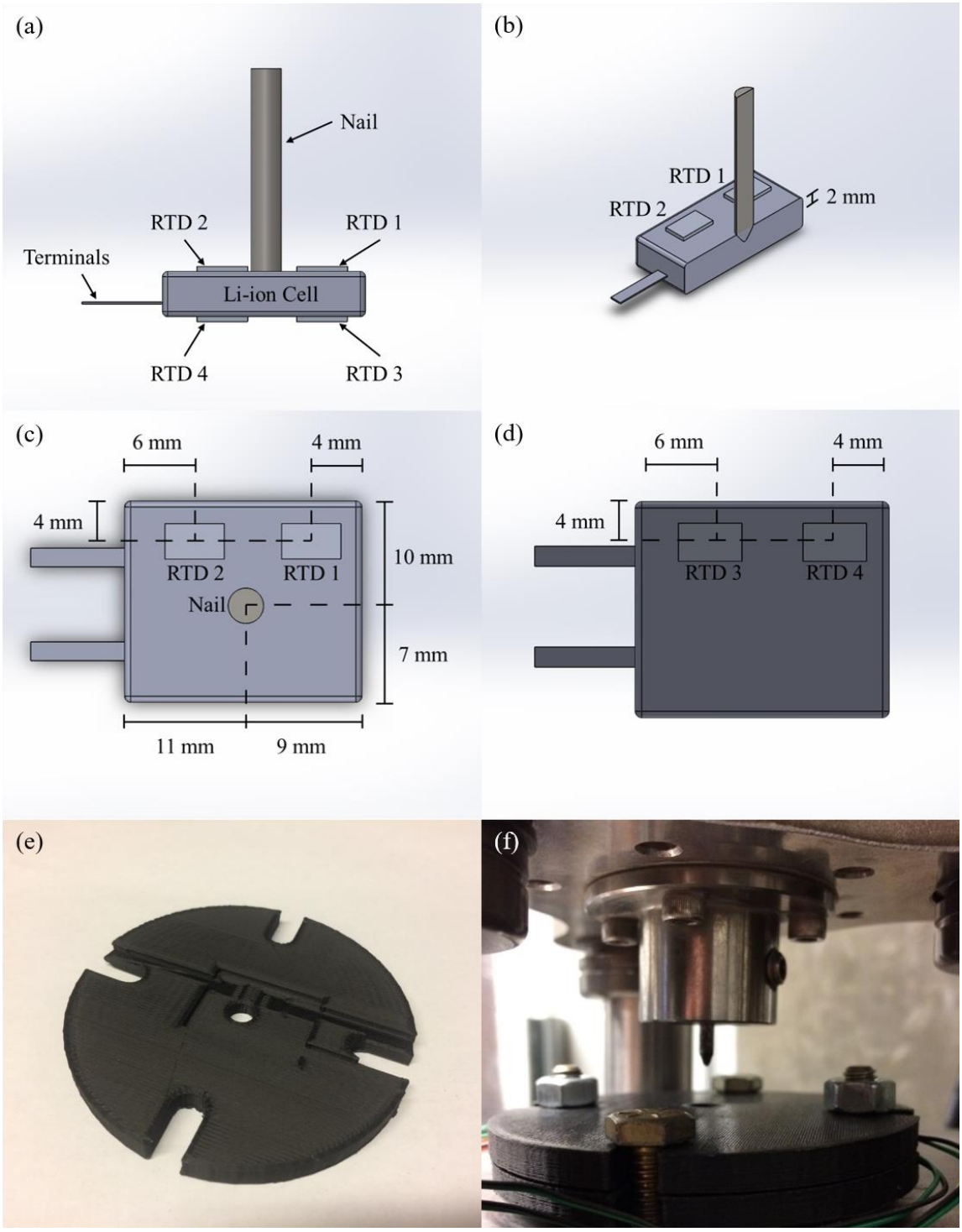

Figure 1. (a) Side view of cell with placement of RTDs and location of nail upon impact; (b) Cutaway view showing approximate depth of puncture; (c) Dimensions of RTD placement on top of cell and location of puncture; (d) Dimensions of RTD placement on bottom of cell. (e) Holder with recessed areas for cell and RTD placement, as well as a hole in the center for the nail impact; (f) Placement of holders containing cell and RTDs on test rig underneath the drop hammer with nail inserted.

The experiment implemented a drop hammer test rig in order to puncture the cells with the nail. A steel nail was attached to the hammer, and rubber shims were placed at the bottom of the rig to maintain the puncture depth of the nail into the battery at 2 mm. The battery was cycled using a battery analyzer (from AA Portable Power Corp.) which also recorded the voltage, current, capacity, and coulombic efficiency of the battery throughout the tests.

The battery and RTDs were placed inside the holders and bolted together, then secured in the test rig below the hammer. Fig. 1 (e, f) show the holder used to secure the cell and RTDs, and the placement of the holders on the test rig. The hammer was held in position using a magnetic hoist and placed at a height where the tip of the nail was 10 mm above the center of the battery, limiting the momentum and depth of the puncture to prevent the onset of thermal runaway.

3.3.2 Testing Procedure

Each cell was connected to the cycler/analyzer and charged to its charge cut-off voltage of 4.2 V, then discharged to its discharge cut-off voltage of 3.0 V and allowed to rest for 1 minute after each full cycle. The charges and discharges were performed at the maximum charging current of 170 mA.

The battery cycler/analyzer performed 15 charge cycles and 14 discharge cycles to obtain baseline operational data for the cycle times, capacity, coulombic efficiency, and external temperatures prior to the puncture. When the cell reached 4.2 V at the end of charging on the 15^{th} cycle, the hammer was released and the nail impacted the cell at 100% state of charge (SOC). Fig. 2 (a, b) show the physical damage to a cell caused by the nail puncture.

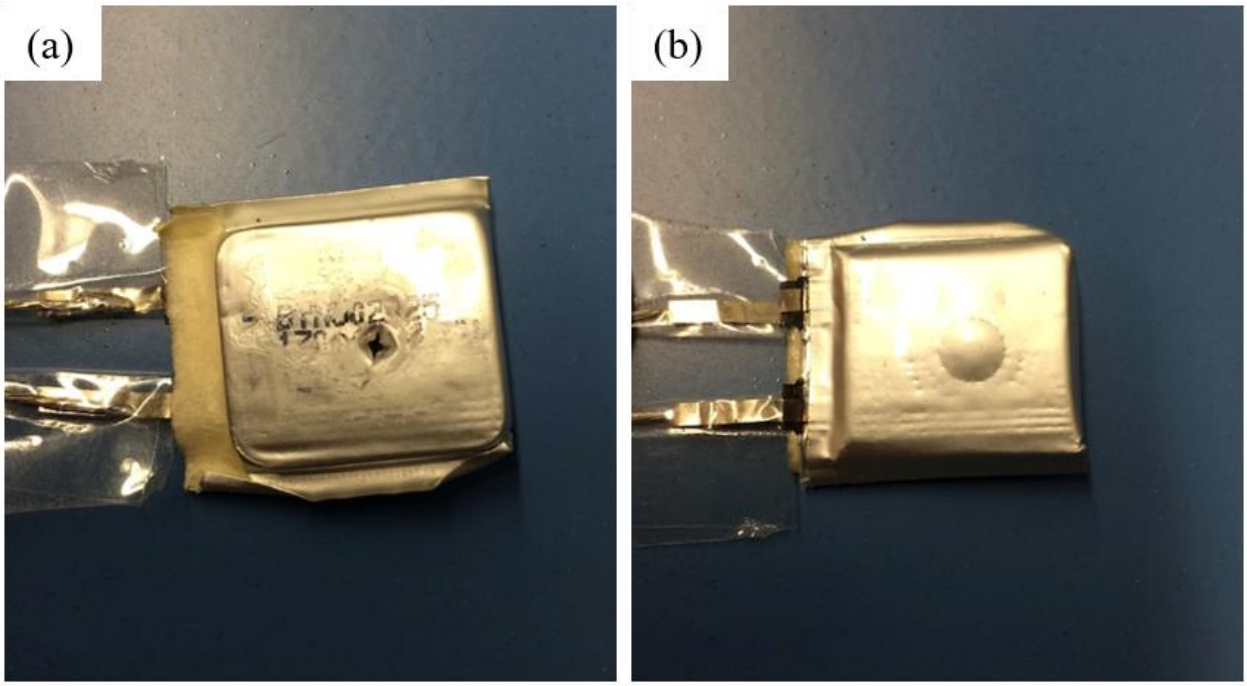

Figure 2. (a) Puncture on top side of cell after impact; (b) Protrusion on bottom side of cell after impact.

After the puncture occurred, the hammer was raised to remove the nail from the cell for the remainder of the test and no smoke or combustion were observed. Since the nail did not completely penetrate the cell, it was not fully shorted as in the conventional nail penetration tests and retained to ability to continue cycling. The cell was left attached to the battery analyzer to continue performing another 84 charge/discharge cycles to obtain the same operational information as before the puncture. Table 3 shows the different groups of cycles and their reference to the impact.

Table 3: Timeline of charge and discharge cycles in relation to impact from nail.

Cycle(s)	Time in relation to impact
1-14	Full cycles before impact
15 (charging)	Final full charge before impact
15 (discharging)	Impact
16 (charging)	Partial charge after impact
16 (discharging)	First full discharge after impact
17-100	Full cycles after impact

A total of 100 cycles were completed to determine how long a cell would continue operating after a nail puncture prior to reaching its EOL. Cycle 15 did not complete a full charge/discharge since the impact occurred at the end of the charge cycle and the cycling was interrupted by the PCM due to the impact. Cycle 16 did not complete a full charge/discharge cycle because the voltage for the charge began at approximately 3.9 V for each cell from the incomplete discharge of cycle 15. Because the information from these cycles is incomplete, the data for analysis is split into two groups: cycles 1-15 before impact, and cycles 17-100 after impact.

In order to verify the results observed and the conclusions determined after analysis, two other cells were used in this experiment. The first cell was cycled normally without a nail puncture to provide control data. The second cell implemented the same cycling and nail puncture procedure, but a piece of electrical tape was applied as soon as possible to cover the puncture in order to minimize the amount of water vapor and other contaminants that could enter the exposed cell.

3.4 Results

3.4.1 Physical Effects of Nail Puncture on LIBs

Upon disassembly of the cells, it was determined that the nail penetrated through five of the ten anode/separator/cathode layers of each cell. An approximation of the amount of electrode coating removed for the first layer of the penetration was 10.5%, based on the area of the electrode layer and the area of the hole caused by the nail. Fig. 3 (a-c) show the anode, separator, and cathode at the location of most damage from the puncture after disassembly of one of the cells.

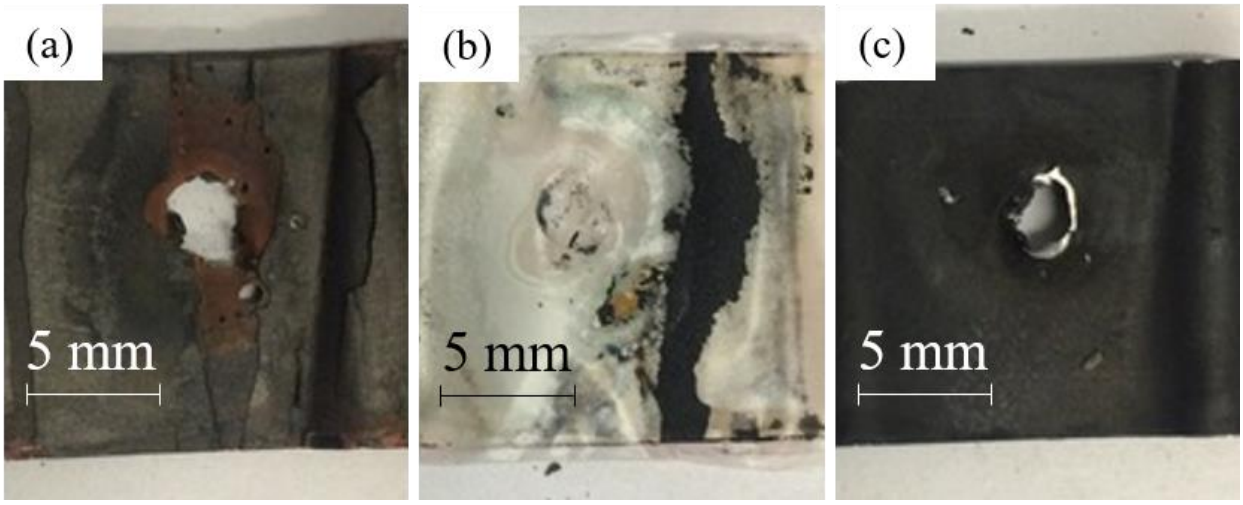

Figure 3. (a-c) The first layer of the anode, separator, and cathode, respectively, of the cell where the nail punctured occurred.

The amount of damage for each component was different, and the extent of the damage lessened for each layer that the nail punctured due to the conical tip of the nail. On the anode large amounts of the graphite coating were removed from the foil near the penetration, which can be seen by the visible copper around the edges of the puncture. More material is lost on the anode than the cathode due to the graphite coating being brittle and breaking away from the copper foil more easily [30]. The coating removed from the anode also became stuck to the separator due to the high temperatures reached from the impact. The cathode had less material loss from the area around the puncture than the anode, as less of the foil can be seen around the puncture on the cathode.

These results provide some indication as to why the cells did not fully short due to the nail impacts. Previous studies have shown that the severity of a short can be attributed to the amount of damage caused to a cell and its electrode layers; an indentation that does not penetrate a cell can cause a soft short and little to moderate voltage loss, whereas a full nail penetration normally causes a hard short and complete voltage loss [20]. Also, a deeper nail penetration results in a higher amount of shorted electrode layers and a larger region of internal short circuit [22]. Because the puncture in this experiment pierced approximately half the electrode layers, and because removing the nail after the impact also removed the contact between the electrodes, the cells experienced only a momentary short that caused a decrease in voltage but were still able to cycle afterwards.

SEM images of the cathode were obtained at different areas relative to the puncture, as well as from a control cell that was cycled in the same manner that did not experience a nail puncture. Fig. 4 (a) shows the location of the SEM images on the cathode near the puncture, and Fig. 4 (b, c) show the SEM images of the cathode at different locations inside the cell. Fig. 4 (d) shows the SEM image of the cathode from the control cell that was cycled the same number of times as the other cells.

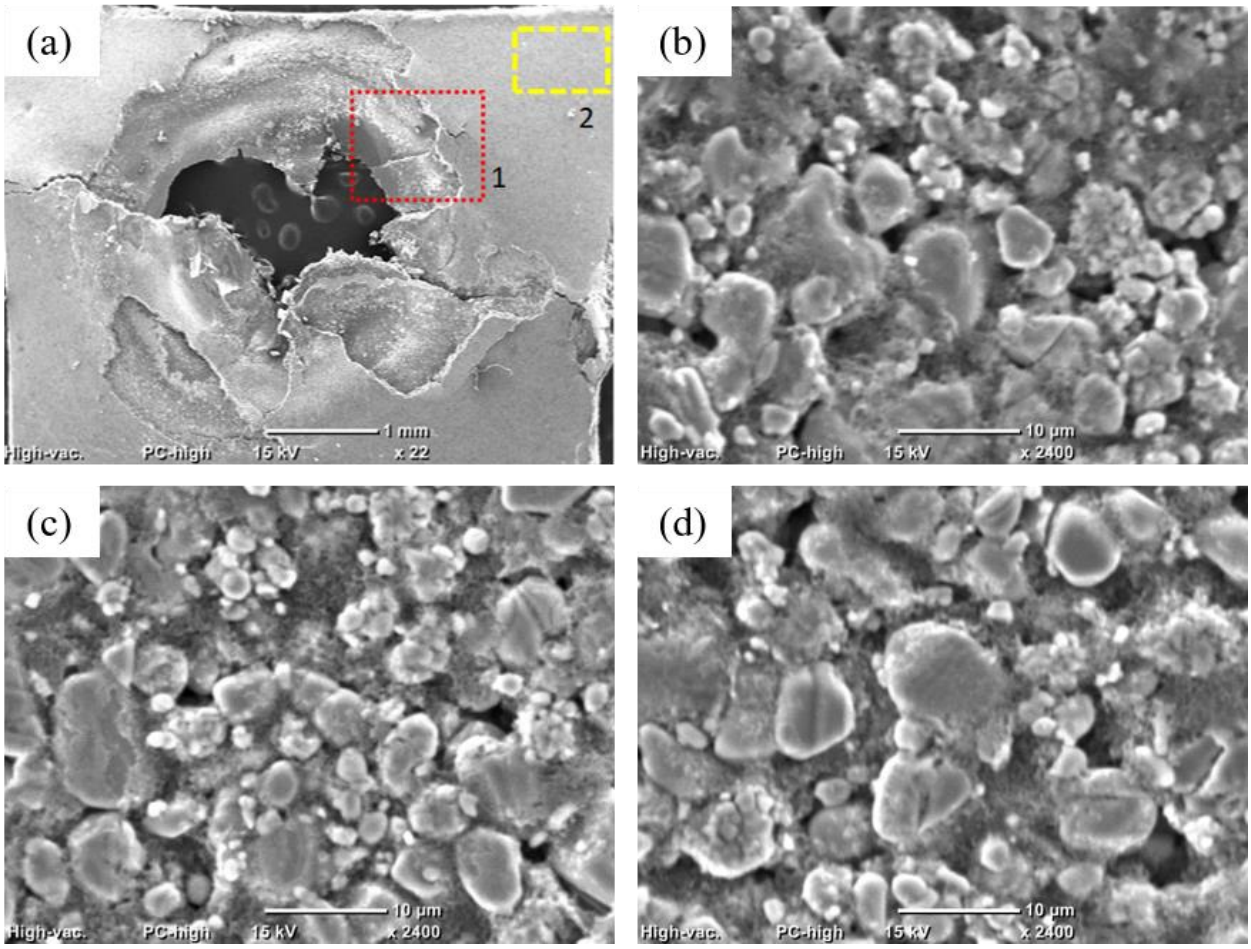

Figure 4. (a) Image of the damage to the first layer of the cathode where the nail was inserted; (b) Image of the cathode particles on the area immediately next to the puncture where the LCO coating had not been removed by the nail (region 1 in image a); (c) Image of the cathode particles approximately 2 millimeters from the site of puncture (region 2 in image a); (d) Image of the cathode particles on the cathode layer of a normally cycled cell with no nail impact.

It was anticipated that the higher temperature caused by the puncture may expedite the agglomeration of cathode particles by sintering that is seen during normal aging of a cell [31, 32]. However, the results from the SEM imaging did not show a distinct difference in the particle size between the cells. While the nail puncture directly affected the cells through the deformation of the casing and removal of material from the cathode and anode, there appeared to be no indirect effect on the cathode material that would also influence the operational performance of the cells. Earlier, mechanical analyses by various researchers have shown that at the loads considered interparticle fracture and intra-particle fracture does not propagate, [33-35].

3.4.2 Effect on LIB Temperature Change

Each LIB exhibited a normal temperature profile during the regular charging and discharging cycles prior to the nail impact [36-38]. The temperatures increased throughout the exothermic discharge cycle, where the peak temperature observed was at the end of the discharge. The lowest temperatures were observed shortly after the discharge cycle and rest period were completed, then temperatures increased again during the charge cycle. When the punctures occurred, the temperatures at each RTD location on the cells increased rapidly, then slowly decreased as the heat dissipated from the casing of the cells. Fig. 5 (a, b) show the temperature behavior of the highest reading RTD of each cell for the puncture which begins when the time is equal to zero, as well as the rate of temperature change in each cell caused by the puncture.

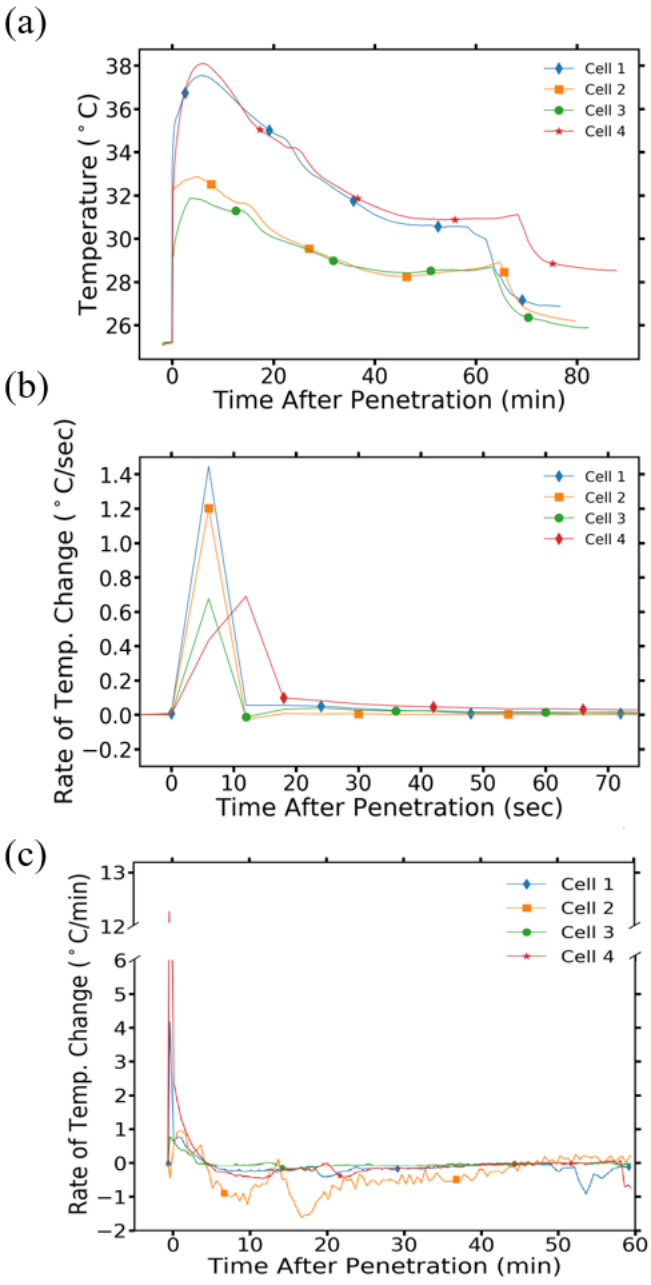

Figure 5. (a) Temperature of the highest reading RTD for each cell during and shortly after nail puncture; (b) Rate of temperature change during initial rise in temperature caused by puncture; (c) Rate of temperature change at a larger scale after nail puncture.

The momentary short circuiting of the electrodes due to being pinched together by the nail puncture resulted in a rapid increase in joule heating and a sharp external temperature rise on the casing of the cells. The rate of temperature increase was highest during the momentary short caused by the pinching of the electrodes due to joule heating, after which the rate decreased to a level just above zero. The temperature on the casing of the cell continued to increase as the rest of the thermal energy was transferred to the casing of the cell. The peak temperatures for each cell were seen at approximately 5-10 minutes after the punctures, at which point the temperatures decreased slowly as the heat from the cell dissipated through convection heat transfer. Since the discharge process is an exothermic reaction, heat was continually added to the cells for approximately one hour after the puncture and the temperature decreased at a slower rate [39]. A steep drop in temperature can be seen in each of the cells approximately 65-75 minutes after the puncture, coinciding with the beginning of the first full charging cycle after the puncture for each of the cells. This abrupt drop in temperature is due to the charge process being an endothermic reaction. This was the first instance after the puncture where thermal energy was not being added and allowed the cell temperatures to decrease more rapidly [40].

3.4.3 Effect on Capacity and Coulombic Efficiency

Prior to the impacts, the charge and discharge capacities for each battery maintained relatively constant values during cycling. After the punctures, the capacity discharged dropped to a level below what had been seen before the punctures, then gradually decreased over the remaining cycles. The capacity charged to each cell rose to a level above what was seen before the punctures, decreased sharply for the first 5-10 cycles after the punctures to near the same value as the capacity discharged, then maintained a gradual decrease just above the level of the capacity discharged. Fig. 6 (a-h) show the charge and discharge capacities of each cell before and after the punctures.

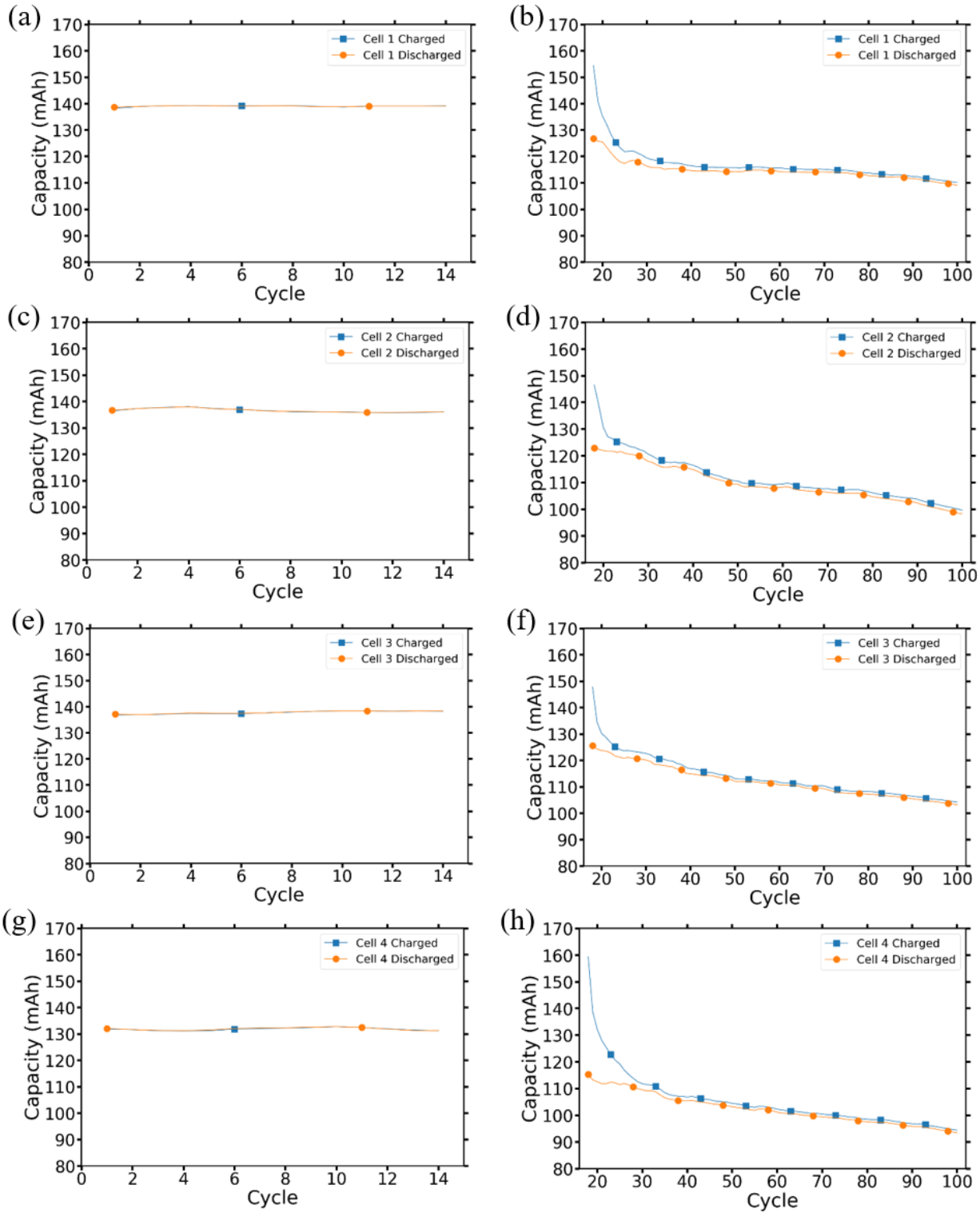

Figure 6. (a-h) The capacity charged and discharged for each cycle before and after the punctures.

The puncture caused an instant drop in discharge capacity of 8.98%, 10.9%, 9.26%, and 13.1% for the first full discharge cycle after the puncture, compared to the maximum discharge capacity prior to impact for cells 1-4, respectively. At the completion of the experiment, a total decrease in capacity of 21.6%, 28.8%, 25.5% and 29.6% from the maximum discharge capacity before impact was seen for cells 1-4, respectively. For the cell that had the puncture covered with electrical tape, there was an initial drop in discharge capacity of 6.43% after the puncture and a drop of 19.9% overall at the completion of the experiment. The cell that was normally cycled without a nail impact saw a decrease in discharge capacity of only 0.8% after 100 cycles. The accelerated decrease in discharge capacity due to the puncture shows each of the cells experienced accelerated aging after the punctures occurred. The aging was accelerated to the point where each of the four tested cells reached 80% of their initial capacity (or EOL) prior to the final cycle of the experiment (the capacity of the cell with tape covering the puncture was slightly above the EOL capacity on the last cycle). The difference in the number of cycles for each cell to reach EOL after the punctures is attributed to small manufacturing differences that cannot be controlled or observed from testing. Fig. 7 (a, b) show the discharge capacity remaining for each cell before and after the puncture. Fig. 7 (b) also shows the discharge capacity remaining for the normally cycled cell and the cell with tape over the puncture.

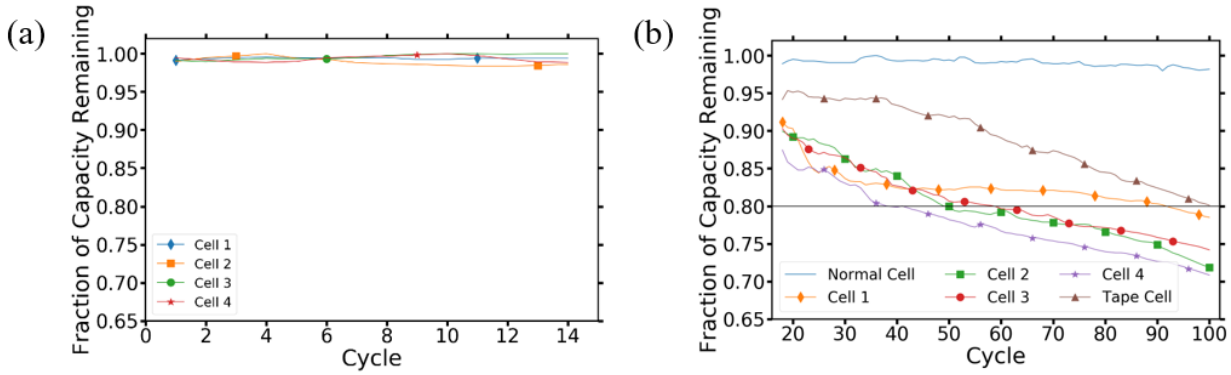

Figure 7. (a) The fraction of capacity remaining for each cell before the punctures; (b) The fraction of capacity remaining for each cell after the punctures compared to the normally cycled cell and cell with tape covering the puncture. EOL is indicated by the line at 0.80, corresponding to 80% of initial discharge capacity.

During normal operation, the coulombic efficiency of a cell is expected to decrease approximately 0.4%-0.6% over the lifetime of a cell due to capacity degradation [41]. For this

experiment, it was observed that the cycle when the nail puncture happened was of low coulombic efficiency. The nail puncture event also affected the cycles after it. For cells 1-4, the coulombic efficiency decreased to 82.1%, 83.9%, 85.0%, and 72.4%, respectively, for the first full cycle after puncture. Then the coulombic efficiency increased to a level just below that seen prior to the puncture (approximately 98.5%-99.1%). Fig. 8 (a, b) show the coulombic efficiency of each cell before and after the puncture, as well as the coulombic efficiency for the normally cycled cell and the cell implementing electrical tape over the puncture in Fig. 8 (b). For the cell that had the puncture covered with electrical tape, there was an initial decrease in coulombic efficiency to 84.6% after the puncture, after which the coulombic efficiency increased to approximately the same final value at the same rate as the other punctured cells.

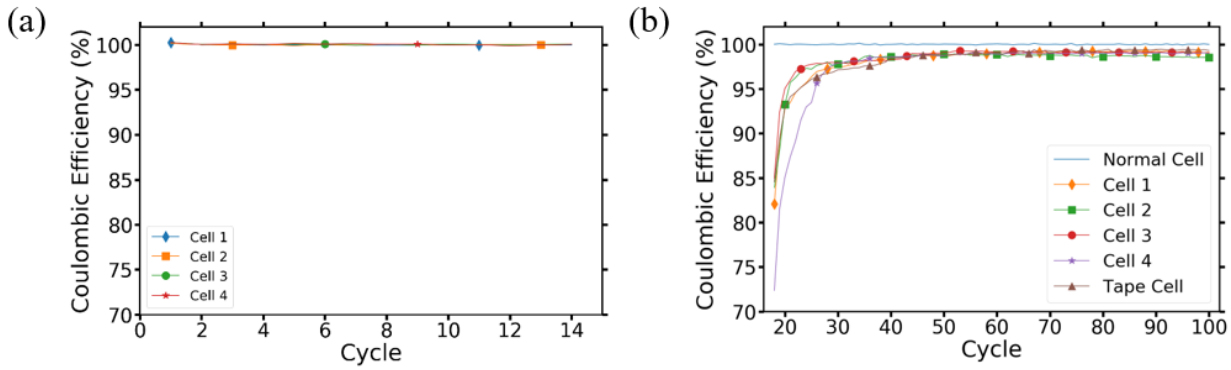

Figure 8. (a) The coulombic efficiency for each cell before the puncture; (b) The coulombic efficiency for each cell after the puncture compared to the normally cycled cell and cell with tape covering the puncture.

The behavior of the coulombic efficiency gives an indication that the damage to the cells caused by the puncture is only temporary and that there may be some type of self-healing effect present. The significant difference in charging and discharging capacities of cycle 16 could be contributed to the removal of electrode active material, which happened when the LIB was fully charged and punctured. The material loss caused a sudden decrease in LIB capacity and was firstly reflected in the first full discharging cycle after the puncture. After that, the material loss started to be reflected in the charging cycles and resulted in instant recovery of coulombic efficiency. The coulombic efficiency continued to rise as the heat generated from nail puncture dissipated and LIB temperature returned to its normal range. Although the coulombic efficiencies stabilized at around

98% within 10-15 cycles after the puncture and continued to slightly improve afterward, both the capacity charged and capacity discharged decreased at essentially the same rate beginning at that time.

3.4.4 Effect on Incremental Capacity

Prior to the puncture, each cell exhibited a typical incremental capacity profile for LIBs under correct operation. After the puncture occurred, the incremental capacity profile changed in multiple ways: the starting voltage for each charge cycle increased which could be contributed to an increase in internal resistance; the maximum incremental capacity for each cycle initially jumped then decreased as the number of cycles after the puncture increased; and the final incremental capacity value at the end of each cycle increased. Fig. 9 (a-h) show the incremental capacity curves of each cell throughout the entire experiment. A reliable method for producing incremental capacity curves without the need for smoothing, known as the LEAN method, has been proposed in a previous work [42]. This method could not be implemented on the data obtained for these experiments due to the difference in sampling rate but would provide an accurate method of representing the data.

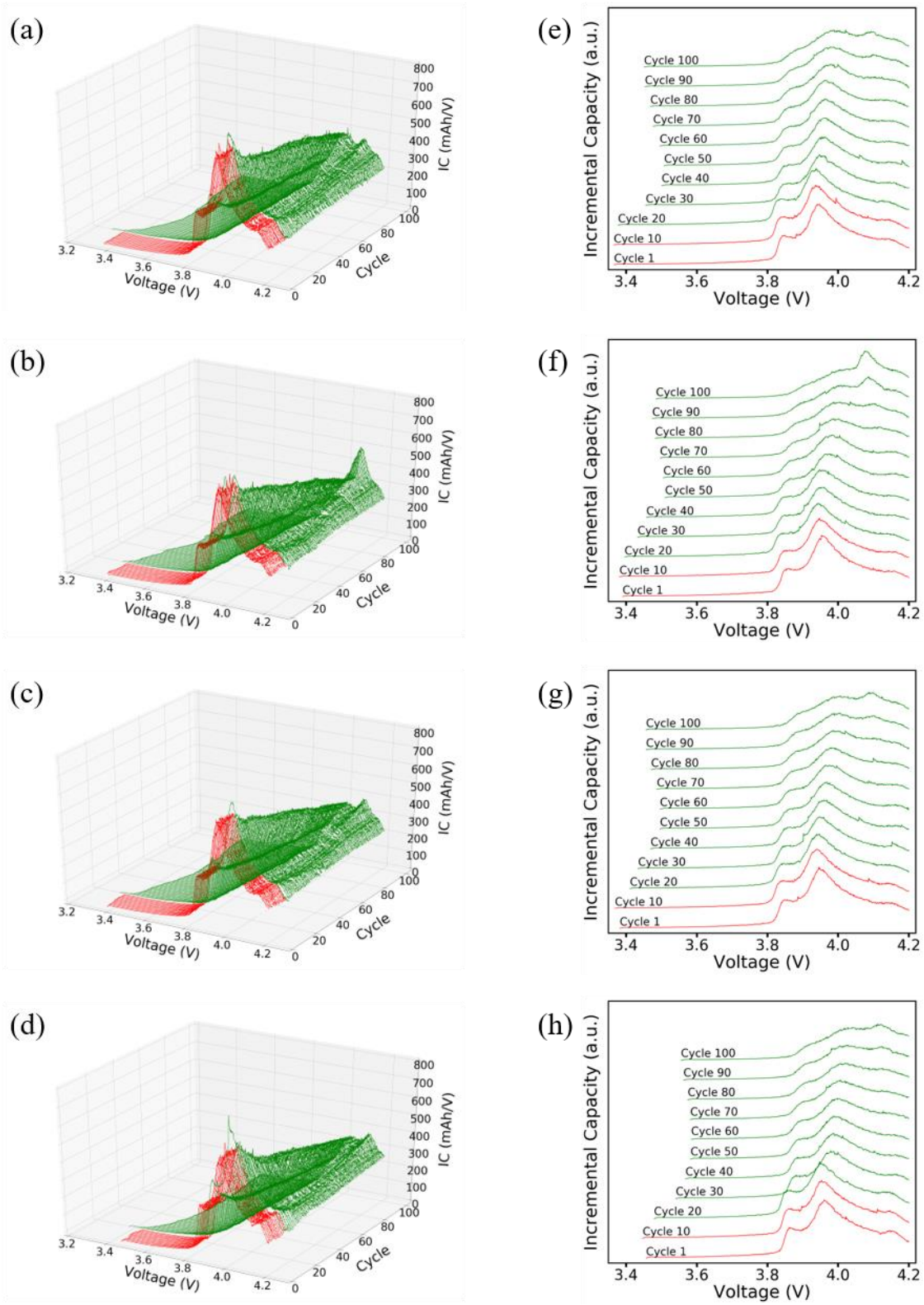

Figure 9. (a-d) Incremental capacity curves for cells 1-4, respectively. The red curves are cycles 1-15 which occurred before the puncture, and the green curves are cycles 17-100 which occurred after the puncture; (e-h) The same results provided using a two-dimensional representation.

The most significant effect on the incremental capacity was the gradual decrease in the maximum value after the puncture occurred. The decrease in the maximum incremental capacity per charge cycle corresponded to the decrease in the discharge capacity of the cells after the punctures occurred. The effects on incremental capacity indicate that the punctures caused each of the cells to experience accelerated aging. This outcome is analyzed in the following section.

3.5 Discussion

The first change in the operational capacity of the cell immediately followed the impact. Initially the charge capacity rose for each of the cells by a range of 6-20%, then decreased during the ensuing cycles. The largest increases in charge capacity were seen in cells 1 and 4, which were the cells that had the higher peak and operating temperatures immediately following the nail puncture. The charge capacities then decreased during the ensuing cycles until they were near the same value as the discharge capacities, which took approximately 10-15 cycles. The increase in charge capacity is attributed to the operation at higher temperatures, which causes a short-term increase in performance and an increase in charge capacity. An increase in ambient temperature from 25°C to 55°C results in a charge capacity increase of approximately 20% [43]. The largest capacity increase seen in a punctured cell was 20% with a peak casing temperature of 38°C. Because the internal temperature of the punctured cells is higher than the external temperature, these results are plausible. Operating at a higher temperature also increases the degradation rate, which is exhibited by the decrease in charge capacity that occurs after the puncture. Also, a sudden decrease in discharge capacity was seen in each cell during the first full cycle after the puncture, with a capacity loss in the range of approximately 9-13%. This can be attributed directly to the immediate physical damage from the impact presented in Fig. 2,3. As seen in Fig. 3 (c) and Fig. 4 (a), the nail removed material from the electrodes resulting in less active lithium being available. Because of this loss of material, an immediate drop in the discharge capacity of the cells occurred. After this initial drop, the capacity continued to decrease at an approximately constant rate for most of the cells. While the manufacturer specifies that the lifetime of the cells is at least 500 cycles, the cells under test each reached their EOL capacity at an average of 59 cycles, or 43 cycles after impact. This long-term fade in capacity is likely due to accelerated aging of the cells caused by the punctures. For the cell that had the puncture covered with electrical tape, the effect on discharge capacity was slightly different. While the discharge capacity initially decreased from the

puncture, it stayed relatively constant for approximately 20 cycles after the puncture before decreasing in the same fashion as the other cells. This cell also did not reach its EOL prior to the conclusion of cycling for the experiment but would have after one more cycle assuming the same trend of discharge capacity decrease had continued.

Typically, a cell ages due to a collection of different mechanisms. The most common forms of aging are conductivity loss (CL), loss of lithium inventory (LLI), and loss of active material (LAM), and there are multiple ways each type of aging occurs. CL occurs due to the degradation of the electronic components and decomposition of the binder, LAM occurs due to structural transformations in the active material and electrode decomposition, and LLI occurs due to variances in the number of lithium ions and decomposition of the electrolyte [44]. Aging causes many chemical reactions to take place within a cell. The continuous intercalation and deintercalation of lithium ions cause a phase change in the LCO to a cubic spinel phase, leading to a loss of cyclable lithium [45]. Parasitic chemical reactions at the electrode-electrolyte interface also lead to a loss of electrons and lithium ions, as well as the degradation of electrolyte solvents [46]. These factors lead to increased internal resistance and decreased electrical conductivity from a decrease in the effective surface area of the cathode particles, leading to a decrease in capacity as well as a compromised ability to recharge [47]. The extent of each of these aging mechanisms are uniquely variable in all cells and have been shown to be independent of initial variations between cells, showing that monitoring an individual cell's state of health during operation is non-trivial [48].

These methods of degradation are compounded by multiple reactions that occur when the internal components of the cell are exposed to atmosphere from the nail puncture. When the lithium hexafluorophosphate ($LiPF_6$) present in the electrolyte interacts with water vapor in the atmosphere, hydrogen fluoride (HF) is created. This causes decomposition and reduces the conductivity of the electrolyte, leading to decreased performance of a cell [49-52]. Also, the exposure to atmosphere combined with operation at higher temperatures resulted in the release of oxygen from the cathode materials. Oxygen release in cells results in structural degradation and a rapid fade of capacity, leading to a reduction in performance [53, 54]. This also increases the likelihood of thermal runaway due to a reduction in structural stability. For the cell that had the puncture covered with electrical tape, only a small amount of water vapor from the atmosphere was able to enter the cell before the tape was applied. Because of this, a delay in the reduction of

discharge capacity was observed when compared to the other cells. This behavior could also be attributed to the fact that this cell was less damaged by the nail puncture than the others, as its initial reduction in capacity due to the puncture is lower.

The degradation methods causing aging in the cells under test can be substantiated by analyzing the effects on the incremental capacity curve. The peaks of the curve correspond to the active material chemical and structural evolution, with the largest peak corresponding to the total loss of capacity due to aging of the cell [53-55]. Aging in a cell will cause its incremental capacity curve to shift, usually occurring linearly as the number of cycles increases. This is useful for cell state of health estimation, and tracking the peaks of the incremental capacity curve has been shown to predict capacity fade with low error [54-60]. Each type of degradation will also cause the curve to shift in a distinct manner. CL will normally cause the peaks to shift towards lower voltages, LLI will normally cause the height of the peaks to decrease and shift to either lower or higher voltages, and LAM will normally cause the height of the peaks to decrease without a shift in voltage [44].

By tracking the peak incremental capacity value, as well as the voltage at which it occurs each cycle, the type of aging can be determined for the cells under test. As seen in Fig. 9 (a-d), the peak incremental capacity value for each cell was relatively constant prior to the puncture, jumped slightly immediately after the puncture, then began decreasing. The peak value for the incremental capacity of the cell that had the puncture covered with electrical tape exhibited the same delayed response that was seen for its discharge capacity. Fig. 10 (a, b) show more clearly the maximum incremental capacity values before and after the punctures. Fig. 10 (b) also includes the incremental capacity of the cell with electrical tape over the puncture.

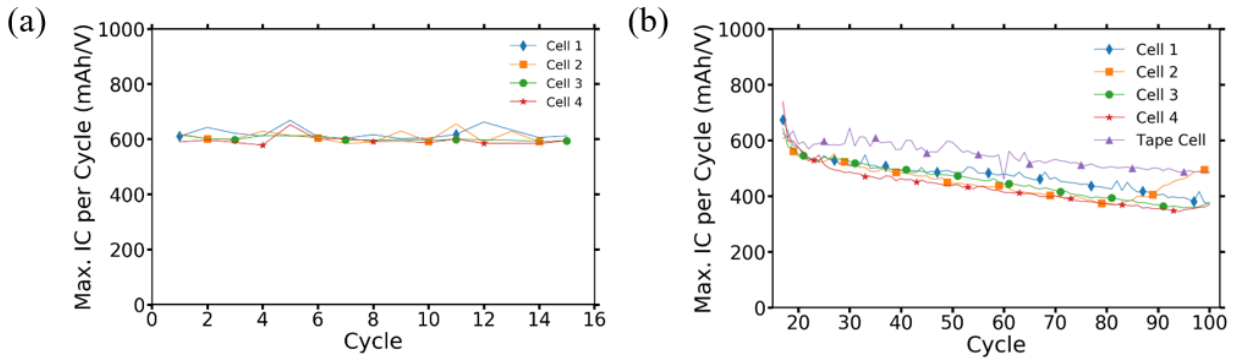

Figure 10. (a) Maximum incremental capacity value per cycle before the punctures; (b) Maximum incremental capacity value per cycle after the punctures compared to the cell with tape covering the puncture.

The peak incremental capacity value for each cell increased slightly for the first full cycle after the puncture, decreased quickly over the next 3-5 cycles, then decreased linearly over the remaining cycles. The peaks of the incremental capacity curves also dropped to a slightly lower voltage immediately after the puncture, then increased in voltage afterwards. Fig. 11 (a, b) show the voltage corresponding to the peak incremental capacity value for each cell for the cycles before and after the punctures occurred. Fig. 11 (b) also includes the voltage corresponding to the peak incremental capacity of the cell with electrical tape over the puncture. Fig. 12 (a, b) show the incremental capacity curves of one of the cells for four separate cycles at different times before and after the puncture to represent how the incremental capacity curve shifted overall.

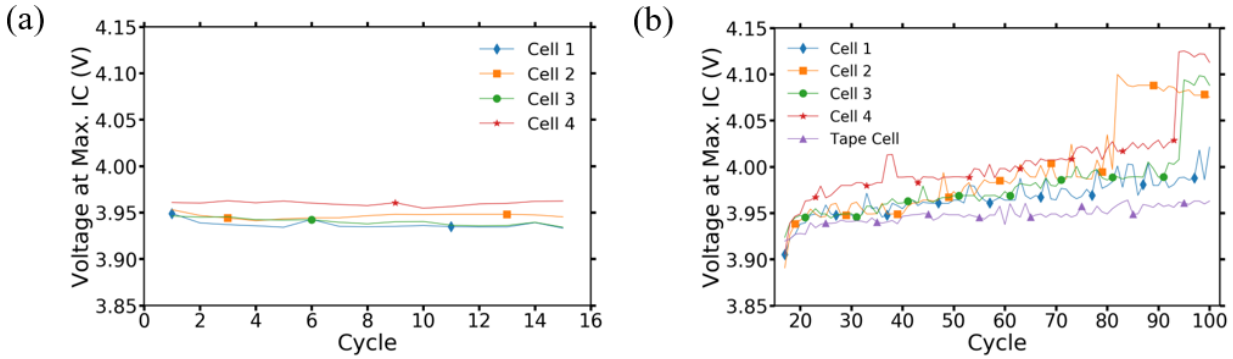

Figure 11. (a) The voltage corresponding to the peak incremental capacity values for each cell before the punctures occurred; (b) The voltage corresponding to the peak incremental capacity values for each cell after the punctures occurred compared to the cell with tape covering the puncture.

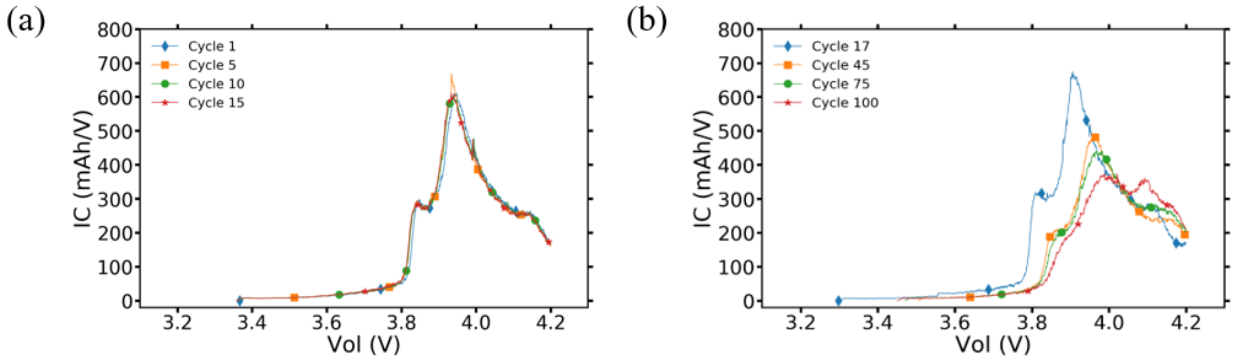

Figure 12. (a) The individual incremental capacity curves for a single cell before the puncture occurred; (b) The individual incremental capacity curves for a single cell after the puncture occurred.

The overall methods of the long-term accelerated aging of the cell are LLI and LAM. LLI has a larger effect during the first few cycles after the nail puncture, and LAM has a larger effect during the cycling afterwards that contributes to the accelerated degradation of the cells. The LLI contribution is determined by the fact that the magnitude of the peaks quickly decreased and the voltage corresponding to the peaks quickly increased during the first few cycles after the nail puncture. The voltage corresponding to the peaks also jumped to a lower voltage immediately after the nail penetration. The shift to LAM is seen as the decrease for the peak magnitude and the increase of their corresponding voltages both decrease their rate of change after the first few cycles [45, 51]. It can be seen that the magnitude of the IC curve during the first cycle after the puncture increased, which is due to the increased charge capacity that is associated with higher operating temperatures for the first few cycles after the puncture.

The impact exposed the internal components of the cell to the atmosphere and led to electrolyte oxidation and eventual decomposition, resulting in LLI. For the cell with tape over the puncture, the oxidation and decomposition were slowed since the addition of water vapor was limited. The physical damage to the electrodes as well as the high temperatures caused by the puncture also resulted in deterioration of the electrodes, which contributed to both LLI and LAM [44, 58]. One unanticipated result was the sudden jump in the voltage corresponding to the peak incremental capacity value near the end of the experiment, which Fig. 11 (b) shows occurred in three of the four cells. This was due to the fact that the maximum incremental capacity value shifted from one peak of the curve to another near the end of the experiment. This phenomenon is possibly due to morphology changes in the cell and will be studied more closely in the future.

3.6 Conclusion

The results of the experiment show that while a LIB is capable of continued operation after being partially damaged, the length of time before it reaches its EOL is drastically reduced. The physical damage to the cells caused an immediate reduction in capacity and cycling efficiency, and initiated the accelerated degradation of multiple components of the cells. Exposure to atmosphere caused a loss of electrolyte due to catalyzation to hydrogen fluoride, as well as oxidation and degradation of the internal components of the cells. Normal mechanisms of cell aging also contributed to the degradation of the cells, causing the amount of lithium available for intercalation and deintercalation to decrease over time. The rise in temperature can also contribute

to the degradation of the electrolyte and electrodes of the cell. These factors caused a decrease in capacity and an increase in internal resistance, which hindered the ability of the cell to charge and discharge properly, and greatly shortened its useful lifetime. It was also seen that the application of electrical tape over a puncture immediately after impact has the ability to slow the degradation of a cell and extend its life by a short amount, but this does not have a significant effect overall.

3.7 Author Contributions

Casey Jones: Conceptualization, Methodology, Validation, Investigation, Data Curation, Writing – Original Draft, Visualization. **Bing Li:** Conceptualization, Methodology, Resources, Writing – Review & Editing, Visualization. **Vikas Tomar:** Conceptualization, Resources, Research result analyses, Writing – Review and Editing, Supervision, Funding Acquisition.

3.8 Acknowledgements

This work was supported by the Office of Naval Research (ONR) [grant number N00014-18-1-2397]. ONR had no direct involvement in this manuscript. The authors would like to thank Dr. Michele Anderson of ONR for her support of this research. We would also like to thank Dr. Vilas Pol and Dhanya Puthusseri of the ViPER Lab at Purdue University for their assistance with the SEM images in this manuscript.

3.9 References

[1] Palacin, M. R., 2009, "Recent Advances in Rechargeable Battery Materials: A Chemist's Perspective," Chemical Society Reviews, **38**, pp. 2565-2575.

[2] Manthiram, A., 2017, "An Outlook on Lithium Ion Battery Technology," ACS Central Science, **3**, pp. 1063-1069.

[3] Abraham, D., 2001, "Lithium Ion Batteries - Materials and Technology," *Presentation at CMM-MRL-UIUC,* Argonne National Laboratory, Lemont, IL.

[4] Wang, H., Lara-Curzio, E., Rule, E., and Winchester, C. S., 2017, "Mechanical Abuse Simulation and Thermal Runaway Risks of Large-format Li-ion Batteries," Journal of Power Sources, **342**, pp. 913-920.

[5] Escobar-Hernandez, H. U., Gustafson, R. M., Papadaki, M. I., Sachdeva, S., and Mannan, M. S., 2016, "Thermal Runaway in Li-ion Batteries: Incidents, Kinetics of the Runaway and Assessment of Factors Affecting Its Initiation," Journal of the Electrochemical Society, **163**(13), pp. A2691-A2701.

[6] Li, B., Adams, R. A., Kazmi, J., Dhiman, A., Adams, T. E., Pol, V. G., and Tomar, V., 2018, "Investigation of Response of $LiCoO_2$ Cathode to Dynamic Impact Using Raman Imaging-Based Analyses," JOM, **70**, 1423-1429.

[7] Lamb, J. Orendorff, C. J., Steele, L. A. M., and Spangler, S. W., 2015, "Failure propagation in multi-cell lithium ion batteries," Journal of Power Sources, **283**, pp. 517-523.

[8] Li, B., Parekh, M. H., Adams, R. A., Adams, T. E., Love, C. T., Pol, V. G., and Tomar, V., 2019, "Lithium-ion Battery Thermal Safety by Early Internal Detection, Prediction and Prevention," Scientific Reports, **9**, 13255.

[9] Adams, R. A., Li, B., Kazmi, J., Adams, T. E., Tomar, V., and Pol, V. G., 2018, "Dynamic impact of $LiCoO_2$ electrodes for Li-ion battery aging evaluation," Electrochemica Acta, **292**, 586-593.

[10] Yuan, L., Dubaniewicz, T., Zlochower, I., Thomas, R., and Rayyan, N., 2020, "Experimental study on thermal runaway and vented gases of lithium-ion cells," Process Safety and Environmental Protection, **144**, pp. 186-192.

[11] Galushkin, N. E., Yazvinskaya, N. N., and Galushkin, D. N., 2018, "Mechanism of Thermal Runaway in Lithium-Ion Cells," Journal of the Electrochemical Society, **165**(7), pp. A1303-A1308.

[12] Bugryniec, P. J., Davidson, J. N., and Brown, S. F., 2020, "Advanced abuse modelling of Li-ion cells – A novel description of cell pressurisation and simmering reactions," Journal of Power Sources, **474**, pp. 228396.

[13] Jia, Y., Uddin, M., Li, Y., and Xu, J., 2020, "Thermal runaway propagation behavior within 18,650 lithium-ion battery packs: A modeling study," Journal of Energy Storage, **31**, pp. 101668.

[14] Williard, N., He, W., Hendricks, C., and Pecht, M., 2013, "Lessons Learned from the 787 Dreamliner Issue on Lithium-Ion Battery Reliability," Energies, **6**, pp. 4682-4695.

[15] Hooper, J.M., and Marco, J., 2014, "Characterising the In-vehicle Vibration Inputs to the High Voltage Battery of an Electric Vehicle," Journal of Power Sources, **245**, pp. 510-519.

[16] *Preliminary Report Highway HWY18FH011,* 2019, National Transportation Safety Board.

[17] Chapin, J. T., Gandhi, P. D., and Brazis, P. W., 2014, "NTSB Battery Nail Penetration Tests: Final Report for 787 Battery (Asset 445) Tested at 15°C, Grounded," Underwriters Laboratories.

[18] Zhao, R., Liu, J., and Gu, J., 2017, "A comprehensive study on Li-ion battery nail penetrations and the possible solutions," Energy, **123**, pp. 392-401.

[19] Wenwei, W., Yiding, L., Cheng, L., Yuefeng, S., and Sheng, Y., 2019, "State of charge-dependent failure prediction model for cylindrical lithium-ion batteries under mechanical abuse," Applied Energy, **251**, 113365.

[20] Lamb, J., and Orendorff, C. J., 2014, "Evaluation of Mechanical Abuse Techniques in Lithium Ion Batteries," Journal of Power Sources, **247**, pp. 189-196.

[21] Chombo, P. V. and Laoonual, Y., 2020, "A review of safety strategies of a Li-ion battery," Journal of Power Sources, **478**, pp. 228649.

[22] Mao, B., Chen, H., Cui, Z., Wu, T., and Wang, Q., 2018, "Failure mechanism of the lithium ion battery during nail penetration," International Journal of Heat and Mass Transfer, **122**, pp. 1103-1115.

[23] *Preliminary Report Highway HWY18FH013,* 2018, National Transportation Safety Board.

[24] *United Nations Global Technical Regulation No. 20,* 14 March 2018, United Nations Economic Commission for Europe.

[25] *SAE J2464: Surface Vehicle Recommended Practice,* November 2009, SAE International.

[26] Doughty, D. H. and Crafts, C. C., *FreedomCAR Electrical Energy Storage System Abuse Test Manual for Electric and Hybrid Electric Vehicle Applications,* August 2006, Sandia National Laboratories.

[27] Saxena, S., Le Floch, C., Macdonald, J., and Moura, S., 2015, "Quantifying EV battery end of-life through analysis of travel needs with vehicle powertrain models," Journal of Power Sources, **282**, pp. 265-276.

[28] Debnath, U. K., Ahmad, I., and Habibi, D., 2014, "Quantifying economic benefits of second life batteries of gridable vehicles in the smart grid," Electrical Power and Energy Systems, **63**, pp. 577-587.

[29] Wood, E., Alexander, M., and Bradley, T. H., 2011, "Investigation of battery end-of-life conditions for plug-in hybrid electric vehicles," Journal of Power Sources, **196**, pp. 5147-5154.

[30] Wang, H., Wakings, T. R., Simunovic, S., Bingham, P. R., Allu, S., and Turner, J. A., 2017, "Fragmentation of copper current collectors in Li-ion batteries during spherical indentation," Journal of Power Sources, **364**, 432-436.

[31] Nagpure, S. C., Babu, S. S., Bhushan, B., Kumar, A., Mishra, R., Windl, W., Kovarik, L., and Mills, M., 2011, "Local electronic structure of $LiFePO_4$ nanoparticles in aged Li-ion batteries," Acta Materialia, **59**, 6917-6926.

[32] Ramdon, S., and Bhushan, B., 2014, "Nanomechanical characterization and mechanical integrity of unaged and aged Li-ion battery cathodes," Journal of Power Sources, **246**, 219-224.

[33] Tomar, V., 2008, "Analyses of the role of grain boundaries in mesoscale dynamic fracture resistance of SiC–Si_3N_4 intergranular nanocomposites," *Engineering Fracture Mechanics*, **75** (15), 4501-4512.

[34] Qu, T, Verma, D, Alucozai, M, and Tomar, V, 2008, "Influence of interfacial interactions on deformation mechanism and interface viscosity in α-chitin–calcite interfaces," *Acta Biomaterialia*, **25**, 325-338.

[35] Tomar, V., 2008, "Analyses of the role of the second phase SiC particles in microstructure dependent fracture resistance variation of SiC-Si_3N_4 nanocomposites," *Engineering Fracture Mechanics*, **16** (3), 035001.

[36] Bernardi, D., Pawlikowski, E., and Newman, J., 1985, "A General Energy Balance for Battery Systems," Journal of the Electrochemical Society, **132**(1), pp. 5-12.

[37] Liu, G., Ouyang, M., Lu, L., Li, J., and Han, X., 2014, "Analysis of heat generation of lithium-ion battery during charging and discharging considering different influencing factors," Journal of Thermal Analysis and Calorimetry, **116**, 1001-1010.

[38] Wang, Q., Zhao, X., Ye, J., Sun, Q., Ping, P., and Sun, J., 2016, "Thermal response of lithium-ion battery during charging and discharging under adiabatic conditions," Journal of Thermal Analysis and Calorimetry, **124**, pp. 417-428.

[39] Vazquez-Arenas, J., Gimenez, L. E., Fowler, M., Han, T., and Chen, S., 2014, "A rapid Estimation and sensitivity analysis of parameters describing the behavior of commercial Li-ion batteries including thermal analysis," Energy Conversion and Management, **87**, 472-482.

[40] Shadman Rad, M., Danilov, D. L., Baghalha, M., Kazemeini, M., and Notten, P. H. L., 2013, "Adaptive thermal modeling of Li-ion batteries," Electrochimica Acta, **102**, 183-195.

[41] Yang, F., Wang, D., Zhao, Y., Tsui, K., and Bae, S. J., 2018, "A study of the relationship between coulombic efficiency and capacity degradation of commercial lithium-ion batteries," Energy, **145**, 486-495.

[42] Feng, X., Merla, Y., Weng, C., Ouyang, M., He, X., Liaw, B. Y., Santhanagopalan, S., Li, X., Liu, P., Lu, L., Han, X., Ren, D., Wang, Y., Li, R., Jin, C., Huang, P., Yi, M., Wang, L., Zhao, Y., Patel, Y., and Offer, G., 2020, "A reliable approach of differentiating discrete sampled-data for battery diagnosis," eTransportation, **3**, 100051.

[43] Leng, F., Tan, C. M., and Pecht, M., 2015, "Effect of Temperature on the Aging rate of Li Ion Battery Operating Above Room Temperature," Scientific Reports, **5**(1), pp. 12967.

[44] Pastor-Fernandez, C., Uddin, K., Chouchelamane, G. H., Widanage, W. D., and Marco, J., 2017, "A Comparison between Electrochemical Impedance Spectroscopy and Incremental Capacity-Differential Voltage as Li-ion Diagnostic Techniques to Identify and Quantify the Effects of Degradation Modes within Battery Management Systems," Journal of Power Sources, **360**, pp. 301-318.

[45] Svens, P., Eriksson, R., Hansson, J., Behm, M., Gustafsson, R., and Lindbergh, G., 2014, "Analysis of aging of commercial composite metal oxide – $Li_4Ti_5O_{12}$ battery cells," Journal of Power Sources, **270**, 131-141.

[46] Kim, D., Kang, J., Eom, T., Kim, J., Lee, J., and Won, C., 2018, "An Adaptive Rapid Charging Method for Lithium-ion Batteries with Compensating Cell Degradation Behavior," Applied Sciences, **8**(8), 1251.

[47] Muhlbauer, M. J., Dolotko, O., Hofmann, M., Ehrenber, H., and Senyshyn, A., 2017, "Effect of fatigue/aging on the lithium distribution in cylinder-type Li-ion batteries," Journal of Power Sources, **348**, pp. 145-149.

[48] Devie, A., Baure, G., and Dubarry, M., 2018, "Intrinsic Variability in the Degradation of a Batch of Commercial 18650 Lithium-Ion Cells," Energies, **11**, 1031.

[49] Bi, Y., Wang, T., Liu, M., Du, R., Yang, W., Liu, Z., Peng, Z., Liu, Y., Wang, D., and Sun, X., 2016, "Stability of Li2CO3 in cathode of lithium ion battery and its influence on electrochemical performance," RCS Advances, **6**, 19233.

[50] Stich, M., Gottlinger, M., Kurniawan, M., Schmidt, U., and Bund, A., 2018, "Hydrolysis of $LiPF_6$ in Carbonate-Based Electrolytes for Lithium-Ion Batteries and in Aqueous Media," Journal of Physical Chemistry, **122**, pp. 8836-8842.

[51] Barlow, C. G., 1999, "Reaction of Water with Hexafluorophosphates and with Li Bis(perfluoroethylsulfonyl)imide Salt," Electrochemical and Solid-State Letters, pp. 362-364.

[52] Sharifi-Asl, S., Lu, J., Amine, K., and Shahbazian-Yassar, R., 2019, "Oxygen Release Degradation in Li-Ion Battery Cathode Materials: Mechanisms and Mitigating Approaches," Advanced Energy Materials, **9**, 1900551.

[53] Nam, K., Bak, S., Hu, E., Yu, X., Zhou, Y., Wang, X., Wu, L., Zhu, Y., Chung, K., and Yang, X., 2013, "Combining In Situ Synchrotron X-Ray Diffraction and Absorption Techniques with Transmission Electron Microscopy to Study the Origin of Thermal Instability in Overcharged Cathode Materials for Lithium-Ion Batteries," Advanced Functional Materials, **23**, pp. 1047-1063.

[54] Plattard, T., Barnel, N., Assaud, L., Franger, S., and Duffault, J., 2018, "Combining a Fatigue Model and an Incremental Capacity Analysis on a Commercial NMC/Graphite Cell under Constant Current Cycling with and without Calendar Aging," Batteries, **5**(1), 36-52.

[55] Dubarry, M., Svoboda, V., Hwu, R., and Liaw, B. Y., 2006, "Incremental Capacity Analysis and Close-to-Equilibrium OCV Measurements to Quantify Capacity Fade in Commercial Rechargeable Lithium Batteries," Electrochemical and Solid-State Letters, **9**(10), A454-A457.

[56] Ouyang, M., Feng, X., Han, X., Lu, L., Li, Z., and He, X., 2015, "A dynamic capacity degradation model and its applications considering varying load for a large format Li-ion battery," *Applied Energy*, **165**, 48-59.

[57] Samad, N. A., Kim, Y., Siegel, J. B., and Stefanopoulou, A. G., 2016, "Battery Capacity Fading Estimation Using a Force-Based Incremental Capacity Analysis," Journal of the Electrochemical Society, **163**(8), pp. A1584-A1594.

[58] Li, Y., Abdel-Monem, M., Gopalakrishnan, R., Berecibar, M., Nanini-Maury, E., Omar, N., van den Bossche, P., and Van Mierlo, J., 2018, "A quick on-line state of health estimation method for Li-ion battery with incremental capacity curves processed by Gaussian filter," Journal of Power Sources, **373**, pp. 40-53.

[59] Feng, X., Weng, C., He, X., Wang, L., Ren, D., Lu, L., Han, X., and Ouyang, M., 2018, "Incremental Capacity Analysis on Commercial Lithium-Ion Batteries using Support Vector Regression: A Parametric Study," Energies, **11**, 2323.

[60] Huang, M., 2019, "Incremental Capacity Analysis-Based Impact Study of Diverse Usage Patterns on Lithium-Ion Battery Aging in Electrified Vehicles," Batteries, **5**, 59.

4. CONCLUSION

The objective of this work was to develop a novel experiment that could be used simulate the operation of a LIB in an abusive environment to determine the effect of non-catastrophic damage on a cell that retains the ability to continue operating. The results from the experiment show that while it is possible for a cell to continue operating after experiencing this type of damage, its operational capabilities and overall lifetime are severely reduced. The main reason for this reduction in operation is the accelerated aging that the puncture causes. Physical damage to the cell causes a loss of capacity due to the removal of active material by the nail puncture, and the exposure of the internal components of the cell promotes faster degradation.

This presents an issue for cells that must operate in these types of abusive environments. Damaged cells can lead to operational problems in the systems that they provide power for, and allowing damaged cells to continue operating can increase the risks of thermal runaway, combustion, and explosion. The results from this work can provide a basis for more rigorous testing standards that incorporate different methods and levels of destructive testing, as well as providing necessary information for establishing improved control systems that can recognize and correct for cells that have been damaged during operation.

The results of the experiments also indicate that much more information can be obtained about cells that are partially damaged and continue operating. Other experiments implementing the same setup and procedure can be applied to cells operating at different environmental temperatures, cells that are at different periods in their lifetime, cells that operate at higher or lower charge/discharge rates, different types of cells, and many other scenarios. The incremental capacity curve also shows a significant amount of change, which will be investigated further in later research. The information that has been obtained so far, as well as the potential information that can be obtained in the future, will be vital to further understanding the operation of different types of Lithium-ion batteries.

5. REFERENCES FOR LITERATURE REVIEW

[1] Mendoza-Hernandez, O. S., Ishikawa, H., Nishikawa, Y., Maruyama, Y., and Umeda, M., 2015, "Cathode material comparison of thermal runaway behavior of Li-ion cells at different state of charges including overcharge," Journal of Power Sources, **280**, pp. 499-504.

[2] Escobar-Hernandez, H. U., Gustafson, R. M., Papadaki, M. I., Sachdeva, S., and Mannan, M. S., 2016, "Thermal Runaway in Li-ion Batteries: Incidents, Kinetics of the Runaway and Assessment of Factors Affecting Its Initiation," Journal of the Electrochemical Society, **163**(13), pp. A2691-A2701.

[3] Geder, J., Hoster, H. E., Jossen, A., Garche, J., and Yu, D. Y. W., 2014, "Impact of active material surface area on thermal stability of LiCoO2 cathode," Journal of Power Sources, **257**, pp. 286-292.

[4] Galushkin, N. E., Yazvinskaya, N. N., and Galushkin, D. N., 2018, "Mechanism of Thermal Runaway in Lithium-Ion Cells," Journal of the Electrochemical Society, **165**(7), pp. A1303-A1308.

[5] Srinivasan, R., Baisden, A. C., Carkhuff, B. G., and Butler, M. H., 2014, "The five modes of heat generation in a Li-ion cell under discharge," Journal of Power Sources, **262**, pp. 93-103.

[6] Finegan, D. P., Darcy, E., Keyser, M., Tjaden, B., Heenan, T. M. M., Jervis, R., Bailey, J. J., Vo, N. T., Magdysyuk, O. V., Drakopoulos, M., Di Michiel, M., Rack, A., Hinds, G., Brett, D. J. L., and Shearing, P. R., 2018, "Identifying the Cause of Rupture of Li-ion Batteries During Thermal Runaway," Advanced Science, **5**(1), 1700369.

[7] Wang, Q., Ping, P., Zhao, X., Chu, G., Sun, J., and Chen, C., 2012, "Thermal runaway caused fire and explosion of lithium ion battery," Journal of Power Sources, **208**, pp. 210-224.

[8] Zhang, J., Lv, D., and Simeone, A., 2020, "Artificial Neural Network-Based Multisensor Monitoring System for Collision Damage Assessment of Lithium-Ion Battery Cells," Energy Technology, **8**(5), 2000031.

[9] Koch, S., Birke, K., and Kuhn, R., 2018, "Fast Thermal Runaway Detection for Lithium-ion Cells in Large Scale Traction Batteries," Batteries, **4**(2), pp. 16-27.

[10] Melcher, A., Ziebert, C., Rohde, M., and Seifert, H., 2016, "Modeling and Simulation of the Thermal Runaway Behavior of Cylindrical Li-ion Cells - Computing of Critical Parameters," Energies, **9**(4), pp. 292-311.

[11] Ren, F., Cox, T., and Wang, H., 2014, "Thermal runaway risk evaluation of Li-ion cells using a pinch-torsion test," Journal of Power Sources, **249**, pp. 156-162.

[12] Yokoshima, T., Mukoyama, D., Maeda, F., Osaka, T., Takazawa, K., Egusa, S., Naoi, S., Ishikura, S., and Yamamoto, K., 2018, "Direct observation of internal state of thermal runaway in lithium ion battery during nail-penetration test," Journal of Power Sources, **393**, pp. 67-74

[13] Ichimura, M., 2007-2009, "The safety characteristics of lithium-ion batteries for mobile phones and the nail-penetration test," *29th International Telecommunications Energy Conference*, The Institute of Electrical and Electronics Engineers, Rome, Italy.

[14] Wang, Q., Shaffer, C. E., and Sinha, P. K., 2015, "Controlling Factor of Cell Design on Large-Format Li-Ion Battery Safety during Nail Penetration," Frontiers in Energy Research, **3**.

[15] Chiu, K. C., Lin, C. H., Yeh, S. F., Lin, Y. H., and Chen, K. C., 2014, "An electrochemical modeling of lithium-ion battery nail penetration," Journal of Power Sources, **251**, pp. 254-263.

[16] Waag, W., Kabitz, S., and Sauer, D. U., 2013, "Experimental investigation of the lithium-ion battery impedance characteristic at various conditions and aging states and its influence on the application," Applied Energy, **102**, pp. 885-897.

[17] Wang, E., Wu, H. P., Chiu, C. H., and Chou, P. H., 2019, "The Effect of Battery Separator Properties on Thermal Ramp, Overcharge and Short Circuiting of Rechargeable Li-Ion Batteries," Journal of the Electrochemical Society, **166**(2), pp. A125-A131.

[18] Adams, R. A., Li, B., Kazmi, J., Adams, T. E., Tomar, V., and Pol, V. G., 2018, "Dynamic impact of $LiCoO_2$ electrodes for Li-ion battery aging evaluation," Electrochemica Acta, **292**, 586-593.

[19] Zhang, Y. C., Briat, O., Deletage, J. Y., Martin, C., Chadourne, N., and Vinassa, J. M., 2018, "Efficient state of health estimation of Li-ion battery under several ageing types for aeronautic applications," Microelectronics and Reliability, **88-90**, pp. 1231-1235.

[20] Zheng, L., Zhu, J., Lu, D. D. C., Wang, G., and He, T., 2018, “Incremental capacity analysis and differential voltage analysis based state of charge and capacity estimation for lithium-ion batteries,” Energy, **150**, pp. 759-769.